



Alkali resistant nanocomposite gel beads as renewable adsorbents for water phosphate recovery

Xuanqi Huang, Wufeng Wu, Yan Xia, Wanbin Li, Yanyan Gong, Zhanjun Li *

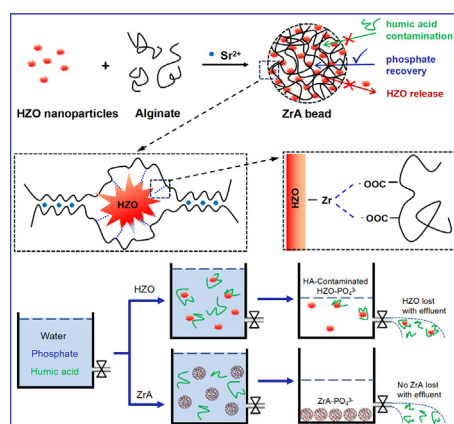
Guangdong Key Laboratory of Environmental Pollution and Health, School of Environment, Jinan University, Guangzhou 510632, China



HIGHLIGHTS

- Hydrous zirconium oxide/alginate beads (ZrA) are prepared for phosphorus recovery.
- Sr^{2+} is the only crosslinking ion that can produce alkali resistant ZrA beads.
- ZrA is mesoporous (15.3 nm) with a specific surface area of $80.84 \text{ m}^2 \cdot \text{g}^{-1}$.
- ZrA shows a high Langmuir adsorption capacity to phosphate ($52.5 \text{ mg} \cdot \text{P} \cdot \text{g}^{-1}$).
- ZrA can be easily recycled and protected from adverse humic acid contamination.

GRAPHICAL ABSTRACT



ARTICLE INFO

Article history:

Received 15 March 2019

Received in revised form 17 May 2019

Accepted 20 May 2019

Available online 21 May 2019

Editor: Huu Hao Ngo

Keywords:

Phosphate recovery

Gel beads

Alginate

Hydrous zirconium oxide

Nanomaterials

ABSTRACT

Hydrous zirconium oxide (HZO) encapsulated alginate gel beads were synthesized for phosphate recovery from water. Importantly, we find that HZO/alginate gel beads (ZrA) crosslinked with Ca^{2+} , Mg^{2+} , Fe^{3+} , Al^{3+} , and Zr^{4+} are unstable under an intense alkali regeneration condition. Only Sr^{2+} -crosslinked ZrA can endure a high alkali solution. ZrA possesses a high specific surface area ($80.84 \text{ m}^2 \cdot \text{g}^{-1}$) and a mesoporous structure (15.3 nm and $0.196 \text{ cm}^3 \cdot \text{g}^{-1}$), which endow them with a high Langmuir adsorption capacity of $52.5 \text{ mg} \cdot \text{P} / \text{g}$. ZrA can be easily recycled, and the mass loss of HZO is prevented. Furthermore, the strontium alginate gel framework protects the encapsulated HZO nanoparticles from adverse humic acid contamination. ZrA can be regenerated for at least 5 adsorption/desorption cycles. Cost analysis indicates the potential scale application feasibility for ZrA. This study provides a novel, simple, and environmentally benign solution to immobilize HZO for efficient phosphate recovery.

© 2019 Elsevier B.V. All rights reserved.

1. Introduction

Phosphorus pollution is among the most important contributors to global water eutrophication, which threatens global aquatic ecosystems and can lead to dramatic economic loss and even damage to human

* Corresponding author.

E-mail address: zjliisci@jnu.edu.cn (Z. Li).

health via cyanotoxin production (Mayer et al., 2016). However, phosphorus is a basic element in all organisms and of critical importance in modern agriculture (Tarayre et al., 2016). However, phosphate ore is a non-renewable resource that will expire in the foreseeable future. Thus, phosphorus recovery from wastewater is not only necessary for aquatic environment protection but also for human sustainable development (Desmidt et al., 2015).

Considerable efforts have been made regarding phosphate removal or recycling from wastewater, for example, the chemical precipitation method of adding calcium or magnesium-rich reagents or materials (Ye et al., 2017). However, most of the existing technologies only work well at high phosphate concentrations. There are still challenges in recycling phosphate at a low concentration. Adsorption is a promising technology for phosphate recovery, as it is easy to handle and cost-effective (Loganathan et al., 2014). Many adsorbents have been developed with a high adsorption capacity; most of these adsorbents are nanomaterials that have a high specific surface area, such as hydrous zirconium oxide nanoparticles (HZOs) (Awual et al., 2011; Chitrakar et al., 2006), iron oxide (Kumar et al., 2017; Othman et al., 2018), MgO (Li et al., 2017; Zhu et al., 2018), lanthanum oxide (Dong et al., 2017; Fang et al., 2017), layered double hydroxides (Everaert et al., 2016), and their composites (Chen et al., 2015; Du et al., 2019; Fang et al., 2018; Qiu et al., 2015; Zhou et al., 2018). HZO is among the best phosphorus recovery materials not only because it possesses a very high adsorption capacity but also because it can be easily regenerated via alkaline washing (Awual et al., 2011; Chitrakar et al., 2006). Although the excellent phosphate removal property of HZO has been proven, several problems remain that hinder its practical applications. First, powder adsorbents are inappropriate for large-scale applications because of the difficulty in separating them during the post-treatment step. It is even more difficult to recycle HZO nanoparticles from water because of their Brownian movement and electrostatic repulsion. Second, the irreversible adsorption of chelating macromolecules (co-existing under natural conditions, such as humic acid) may lead to a dramatic decrease in adsorption capacity. To solve these problems, a number of strategies have been proposed, including loading HZO within porous bulk materials. HZO has been encapsulated in a porous ionic exchange resin and showed outstanding properties for adsorption removal of phosphate, fluoride, arsenic, and so on (Chen et al., 2015; Pan et al., 2014; Zhang et al., 2017). However, a synthetic ion exchange resin is a type of petrochemical that is relatively expensive. A more environmentally benign and cost-effective method is still needed to promote possible HZO applications in phosphorus recovery.

Alginate is a naturally occurring polysaccharide derived from the alkaline digestion of algae or bacteria (Shroff et al., 2018). Alginate can easily form ionic crosslinked alginate gel beads (ALGs) in the presence of multivalent metal ions, such as Ca^{2+} , Sr^{2+} , Fe^{2+} , Fe^{3+} , Al^{3+} , and Zr^{4+} (Fernando et al., 2019). Functional nanoparticles are encapsulated into ALG for diverse environmental applications (Fernando et al., 2019). Meenakshi et al. synthesized ALG crosslinked by Zr(IV) in water defluoridation (Prabhu and Meenakshi, 2015). Jeon and co-workers immobilized zirconium oxide within ALG and successfully utilized it for efficient adsorption removal of As(III), As(V), Cu(II), and Cr(VI) from water (Kumar et al., 2018; Kwon et al., 2016). Lee's group designed Ca^{2+} -crosslinked ALG to encapsulate nano- AlOOH modified biochar for wastewater phosphate recovery applications (Jung et al., 2017). Although many studies have been performed, little effort has been made in phosphate recovery using HZO-encapsulated ALG. The potential influence of ALG on the performance of HZO remains unclear. Furthermore, limited attention has been paid to the regeneration of nanoparticle-encapsulated ALG adsorbents, possibly because of the poor stability of Ca^{2+} -crosslinked ALG under an intense alkali condition, which is needed for adsorbed phosphate desorption.

Inspired by the aforementioned works regarding HZO and ALG, we proposed to encapsulate HZO into ALG beads to produce environmentally benign, alkali resistant and renewable HZO-loaded ALG beads for

phosphorus recovery. SrCl_2 , CaCl_2 , MgCl_2 , FeCl_3 , AlCl_3 , and ZrOCl_2 were used as diverse crosslinking reagents to prepare gel beads, while Sr^{2+} -crosslinked HZO-ALG gel beads (ZrA) were the only stable beads under an intense alkali condition. HZO was immobilized within the ALG hydrogel framework, such that HZO could be easily separated from the treated water while avoiding nano-adsorbent mass loss with the effluent. Furthermore, HZO was shielded from the possible adverse influence of co-existing macromolecules, such as humic acid (HA) (Fig. 1). The influence of the ALG gel on the HZO adsorption properties was studied by determining the ZrA adsorption isotherms and kinetics in comparison to those of HZO. A regeneration experiment was conducted to explore the feasibility of reusing ZrA for multiple phosphate recovery cycles.

2. Experimental

2.1. Materials

Zirconium oxychloride was used as the Zr(IV) source for the HZO. Chemical pure sodium alginate (viscosity, 200 mPa·s) was purchased from Macklin (Shanghai, China). SrCl_2 was used as a crosslinking reagent for sodium alginate gelation. Phosphate solution was prepared by dissolving NaH_2PO_4 . Its concentration was calculated by its phosphorus mass content. NaOH and HCl concentrated acid were used to adjust the pH of the solutions. Ammonium molybdate, antimony potassium tartrate, and ascorbic acid were used in phosphate concentration testing. All the chemicals were A.R. grade unless otherwise stated.

2.2. Synthesis of hydrous zirconium oxide (HZO)

HZO was synthesized using a simple precipitation method. Briefly, a ZrOCl_2 aqueous solution (0.1 M) was prepared. NaOH solution (1 M) was added in a drop-by-drop manner to obtain a pH that was weakly alkaline (pH = 7–8) under vigorous stirring. The mixture was further stirred for 30 min. After ceasing the stirring, the HZO was separated via centrifugation. The supernatant was discarded. Water was added to wash the HZO precipitate to remove additional salt and base, if any. HZO colloidal dispersion (0.1 M, calculated by Zr) was finally obtained by adding water. Its mass concentration was 16.02 g/L tested by weighing the dried HZO powder of a certain volume of HZO colloid. Real-time stirring was performed when HZO dispersion was used for HZO/ALG gel bead synthesis. An HZO powder sample was also prepared via centrifugation and oven drying at 105 °C for 24 h.

2.3. Synthesis of the ZrA beads

Sodium alginate solution (2 wt%) was prepared by dissolving sodium alginate powder into water. Heat was used to facilitate dissolution. The HZO colloidal dispersion and ALG solution were mixed by stirring at a volume ratio of 6:4. $\text{SrCl}_2 \cdot 6\text{H}_2\text{O}$ solution (2 wt%) was prepared as the crosslinking bath solution. A total of 200 mL of the HZO/ALG mixture was dropwise added to 1000 mL of crosslinking bath through a pipette tip at a rate of 2 mL/min. Gel beads were immediately formed when the droplets were immersed into the crosslinking bath solution. Stirring for 1 h was used to complete the gelation reaction. The gel beads were filtered and washed with water three times. The obtained ZrA beads were stored in water at 4 °C. Some ZrA beads were freeze dried and then oven dried at 105 °C for further characterization.

CaCl_2 , MgCl_2 , FeCl_3 , AlCl_3 , and ZrOCl_2 were also used to prepare gel beads according to the same procedure by replacing SrCl_2 .

2.4. Adsorption isotherms of phosphate

To accurately measure the mass of the HZO, dried HZO powder was used for the isotherm. The as-synthesized ZrA beads or HZO (1 g/L) were added to 25 mL of phosphate aqueous solution with diverse

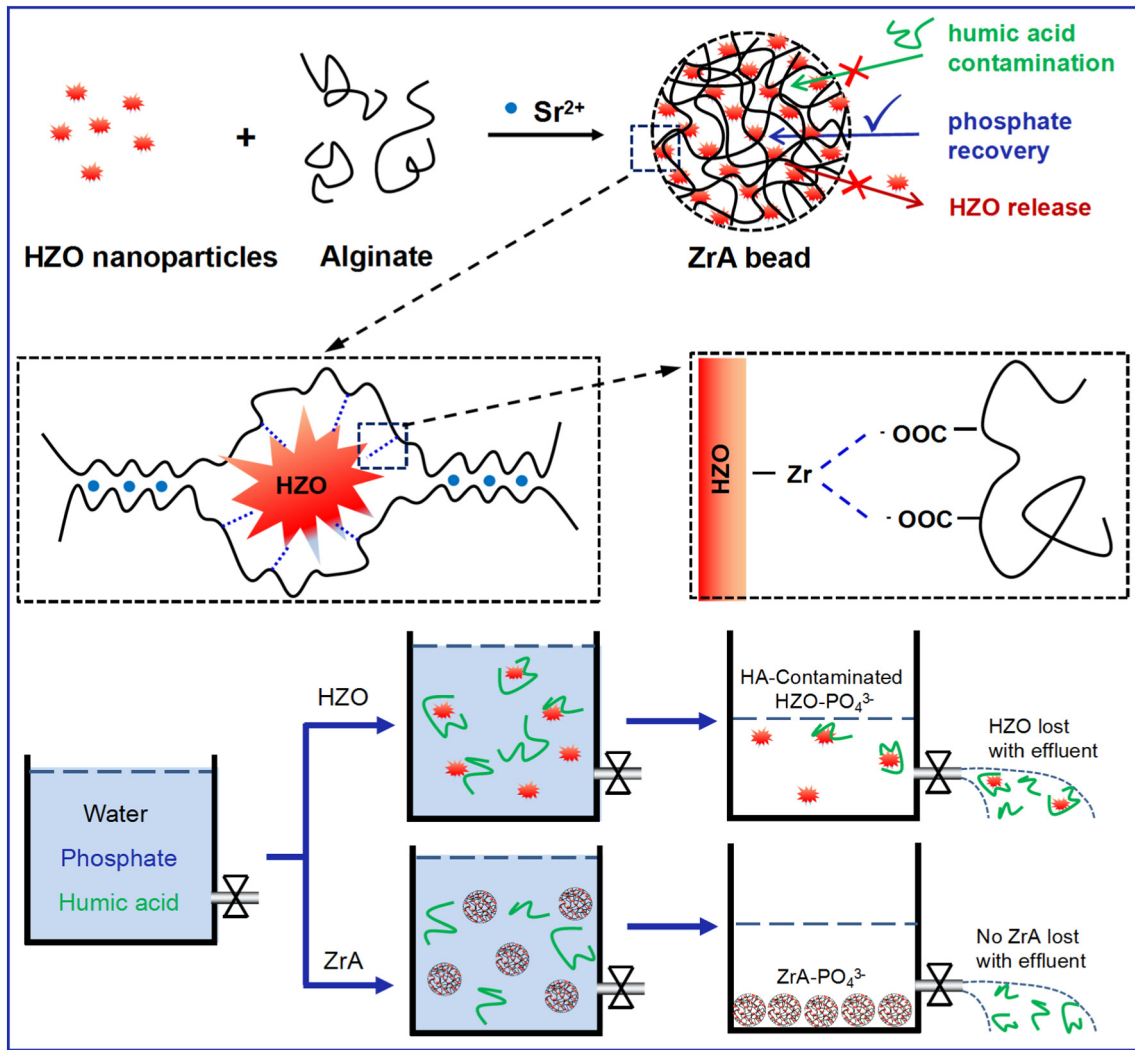


Fig. 1. Schematic illustration of the ZrA gel bead preparation and its application in phosphate recovery.

phosphorus concentrations and shaken for 24 h in a thermostatic oscillator. The phosphate recovery efficiency (η) and equilibrium adsorption capacity (q_e , mg-P/g-adsorbent) were calculated using Eqs. (1) and (2), respectively, as follows:

$$\eta = \frac{(C_0 - C_e)}{C_0} \times 100\% \quad (1)$$

$$q_e = \frac{(C_0 - C_e) \times V}{m} \quad (2)$$

where C_0 (mg/L) is the initial phosphorus concentration, C_e (mg/L) is the equilibrium phosphorus concentration, m (g) is the gel bead dry mass, and V (L) is the phosphate contaminated water volume. The adsorption isotherms were fitted using the following equations:

Langmuir Eq. (3):

$$\frac{1}{q_e} = \frac{1}{q_m k_l C_e} + \frac{1}{q_m} \quad (3)$$

Freundlich Eq. (4):

$$\ln q_e = \frac{1}{n} \ln C_e + \ln k_f \quad (4)$$

where q_e and q_m (mg-P/g-adsorbent) are the equilibrium and max adsorption capacity, respectively; C_e (mg/L) is the equilibrium phosphate concentration and k_l and k_f , n are constants.

2.5. Adsorption kinetics

A total of 0.1 g of ZrA beads (dry mass) or HZO powder was added to 100 mL of phosphate solution (10 mg-P/L) and shaken in a thermostatic oscillator. A 0.2 mL aliquot of the solution was taken for a phosphate test at predetermined time intervals. The equilibrium adsorption capacity (q_e) was measured after 24 h. The adsorption kinetics were fitted using pseudo first-order (Eq. (5)) and second-order (Eq. (6)) models as follows:

$$\ln(q_e - q_t) = \ln q_e - k_1 \cdot t \quad (5)$$

$$\frac{t}{q_t} = \frac{1}{q_e^2 K_2} + \frac{t}{q_e} \quad (6)$$

where q_t and q_e (mg-P/g-adsorbent) are the real-time and equilibrium phosphorus adsorption capacities, respectively; t (h) is the adsorption time; and k_1 (h^{-1}) and k_2 ($\text{g mg}^{-1} \text{h}^{-1}$) are the rate constants of the first and second fitting models, respectively.

2.6. Influence of preloading of humic acid

A total of 0.1 g of HZO powder was dispersed in 500 mL of humic acid solution (0.1 g/L) and stirred for 24 h at room temperature. Humic acid pre-loaded HZO powder (HZO-HA) was obtained after centrifugation and oven dried at 105 °C for 24 h. A 0.5-g HZO control sample (HZO) was obtained using the same procedure without humic acid addition. The mass of the obtained HZO-HA and HZO was measured to calculate the mass loss during the preloading process. HA pre-loaded gel beads (ZrA-HA) were obtained using the same method as that for HZO-HA preparation. The HZO, HZO-HA, ZrA, and ZrA-HA phosphate adsorption capacity were tested using the same method as that for testing the influence of coexisting ions.

2.7. Regeneration of phosphate-adsorbed gel beads

A total of 0.1 g of ZrA was added to 100 mL of phosphate solution (10 mg-P/L) and shaken for 24 h in a thermostatic oscillator. The phosphorus concentration was tested to evaluate the removal efficiency. Phosphate-adsorbed ZrA was placed in 5 mL of NaOH solution (5 wt%) and shaken for 0.5 h in an oscillator at room temperature. After filtration, the gel beads were washed using flowing water to remove the excess NaOH. The residue base was removed via a regeneration solution composed of 0.05 mol/L SrCl₂ and 1 mmol/L HCl. SrCl₂ was used to compensate for the possible metal ion loss during the adsorption process while HCl was used to remove the residue NaOH. Flowing water was again used to wash the gel beads to eliminate the residual Sr²⁺ influence on phosphate adsorption. Regenerated ZrA was finally obtained for the next phosphorus recovery cycle. Five adsorption/desorption cycles were performed to evaluate the ZrA regeneration property.

2.8. Characterizations

To prepare the dried samples for characterization, the gel beads were freeze dried for 3 d and then oven dried at 105 °C for 24 h. The water content of the gel beads and the mean dry mass of the single gel beads were measured and calculated by the mass of 100 wet and dry gel beads. The phosphate concentration (calculated as phosphorus element) was determined using the standard molybdenum blue method (GB11893-89, China) on a UV/VIS spectrophotometer (UV-1780, SHIMADZU, China). The X-ray diffraction (XRD) pattern was acquired using a powder diffractometer with Cu K α radiation ($\lambda = 1.5418 \text{ \AA}$) (D2 PHASER, AXS, Germany). The dried bead microstructures were observed using a field emission scanning electron microscope (FSEM) with an acceleration voltage of 5 kV (S-4800, Hitachi, Japan). The infrared absorption spectra were collected using a Fourier transform infrared (FTIR) spectrometer (IRTracer-100, Shimadzu, Japan). The hydrodynamic size distribution of the HZO nanoparticles was acquired using a dynamic light-scattering device (Zetasizer Nano ZSE, Malvin, UK).

3. Results and discussion

3.1. Alkali resistance of ZrA gel beads using diverse crosslinking ions

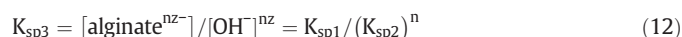
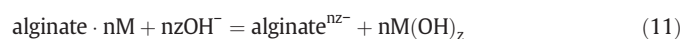
To reduce the economic cost of adsorbents, they should be reusable. Adsorption-saturated HZO regeneration needs to be conducted under an intense alkali condition to desorb phosphate from the HZO particle surface. Thus, ZrA beads should be alkali resistant to ensure successful regeneration such that they can be reused multiple times. We studied the influence of diverse crosslinking reagents on ZrA bead alkali resistance. Interestingly, we found that alginate calcium beads, which are most frequently reported using CaCl₂ to crosslink alginate, are fragile under an alkali condition (NaOH, 1 M, 2 h) and will break into pieces after slight shaking or stirring. We further explored several other multivalent metal ions as potential crosslinking reagents (Table 1). The

Table 1

Alkali resistance (NaOH, 5 wt%, 2 h) of ZrA beads using diverse crossing ions.

Crosslinking reagents	SrCl ₂	CaCl ₂	MgCl ₂	FeCl ₃	AlCl ₃	ZrOCl ₂
Alkali resistance	Stable	Fragile	Broken	Broken	Dissolved	Broken

results indicate that using MgCl₂, FeCl₃, and ZrOCl₂ as crosslinking reagents will generate alginate beads that are unstable under an alkali condition and will be broken after immersion into a NaOH solution even without any shaking or stirring. Using AlCl₃ will generate alginate aluminum beads that can be dissolved into a NaOH solution, possibly because of the amphoteric property of the aluminum ion. Only alginate strontium gel beads using SrCl₂ as crosslinking reagents are stable under an alkali condition. Possible reactions and their corresponding activity products are listed in Eqs. ((7)–(12)) based on the assumption that 1 mol of ALG·nM gel was decomposed into 1 mol of alginate and n mol of metal ions (M^{z+}). The activity product (K_{sp3}) of the gel decomposition reaction (Eq. (12)) has a negative correlation with K_{sp2}, which is the metal hydroxide solubility product constant. We compared the solubility product constants (pK_{sp}) of the corresponding metal hydroxides. The results indicate that Sr(OH)₂ has the smallest value (2.5), several orders of magnitude smaller than that of Ca(OH)₂ (5.3), Mg(OH)₂ (11.7), Fe(OH)₃ (37.4), Al(OH)₃ (32.3), and ZrO(OH)₂ (48.2); thus, ALG-Sr is theoretically the most stable gel. Ca²⁺, Mg²⁺, Fe³⁺, and ZrO²⁺ may lose their crosslinking ability under an alkali condition by forming more stable metal hydroxides. Similar result was found in an existing report showing the advanced stability of ALG-Sr over ALG-Ca (Dechojarassri et al., 2018). The hereafter mentioned ZrA beads were prepared using SrCl₂.



3.2. Physical structures of the as-synthesized ZrA beads

HZO was synthesized by simply precipitating zirconium oxychloride aqueous solution under an alkali condition (pH adjusted by adding NaOH solution) at a size of tens of nanometers (Fig. S1). ZrA gel beads immediately formed after the ALG/HZO colloidal dispersion was added dropwise into the Sr²⁺ solution. The as-synthesized ZrA beads have a uniform spherical morphology with a narrow size distribution of 1.89 ± 0.16 μm (Fig. 2). The milky color is induced by the HZO color. The HZO loading efficiency in ZrA is calculated according to the Zr mass conservation mechanism and the tested dry mass of the obtained ZrA. The optimized HZO content in ZrA is 44.3% under our experiment conditions (Fig. S2). The high HZO loading efficiency in ZrA will ensure a high phosphate recovery capacity. However, further increasing the HZO content will lead to weakening or even breakage of the as-prepared ZrA beads. The XRD patterns of the ALG gel beads, HZO, and ZrA beads show no obvious diffraction characteristics, indicating that the as-synthesized HZO and the HZO encapsulated within ZrA are both amorphous (Fig. S3). The ZrA FTIR absorption spectrum shows a new peak at ~851 cm⁻¹, indicating possible chemical bonding between the ALG carboxyl group and the HZO Zr atom (Fig. S4) (Prabhu and Meenakshi, 2015). This chemical bonding may aid in immobilizing HZO nanoparticles within the gel framework.

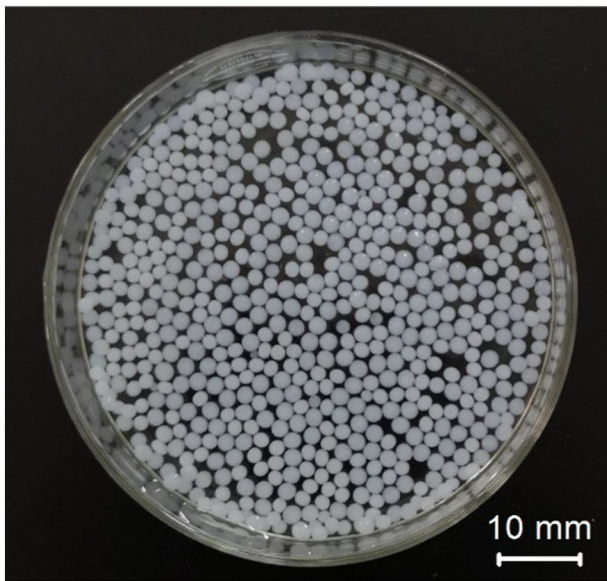


Fig. 2. Optical image of ZrA gel beads.

The microscopic morphology of the ZrA dried gel beads was observed using SEM. The ZrA sample appears as a plump granular (Fig. 3a) and its surface is full of nanoparticles (Fig. 3b). After zooming in on the surface, one can see that the surface contains numerous wrinkles (ALG polymer) and agglomerated nanoparticles (HZO) (Fig. 3c and d). A cross section image was taken along the cutting section (Fig. 3e and f) in which one can see that the ZrA beads contain abundant porous spaces.

The ZrA porous characteristic was further confirmed by the HZO and ZrA N_2 adsorption/desorption isotherms. The HZO and ZrA specific surface areas are $223.2 \text{ m}^2 \cdot \text{g}^{-1}$ and $80.84 \text{ m}^2 \cdot \text{g}^{-1}$, respectively. The hysteresis loops indicate a significant mesoporous character (Fig. 4a). Notably,

the HZO mesopores may more likely be caused by the spaces between adjacent nanoparticles in the HZO dried powder sample. No mesopores exist in the HZO that are larger than 5 nm in diameter (Fig. 4b). Regarding ZrA, mesopores exist within the whole testing range from ~1 to ~24 nm with a mean pore size of 15.3 nm and a pore volume of $0.196 \text{ cm}^3 \cdot \text{g}^{-1}$. The larger pore size is favored to ensure rapid mass transfer during adsorption.

EDX elemental mapping was performed on a cross section. The results shown in Fig. 5 indicate that ZrA contains abundant Zr and Sr elements. Their distributions are generally very uniform within the gel beads at a micrometer scale, possibly benefitting from the stabilization effect of alginate molecules on the HZO distribution. The uniform HZO distribution within ZrA is helpful in maintaining its good adsorption capacity, as severe agglomeration may possibly lead to HZO Ostwald ripening of HZO and in turn a decreased adsorption capacity.

3.3. Phosphate adsorption capacity of the ZrA beads

The ZrA adsorption capacity is evaluated by testing its adsorption isotherm in comparison to that of HZO, which can be better fitted by using the Langmuir model (solid lines) rather than the Freundlich model (dash lines) as shown in Fig. 6 and Table 2. The HZO Langmuir maximum adsorption capacity (q_m) can reach 109.4 mg-P/g. The ZrA q_m is fitted at 52.5 mg-P/g, which is relatively higher not only than other zirconium-based adsorbents, such as commercial zirconium hydroxide (Johir et al., 2016), ZnFeZr nanoparticles (Schneider et al., 2017), Zr/Fe modified carbon fiber (Xiong et al., 2017), HZO-loaded D201 resin (Chen et al., 2015) and Zr/Fe modified 1402 resin (Zhou et al., 2018), but also higher than the reported alginate-encapsulated AlOOH/biochar/ALG gel beads (Jung et al., 2017) and Al-bentonite/ALG beads (Pawar et al., 2016), as shown in Table 3. The possible reason for the higher q_m could be the high specific surface area ($80.84 \text{ m}^2 \cdot \text{g}^{-1}$), mesoporous structure, and high HZO loading efficiency in ZrA (44.3%, Fig. S2). Although Zr-modified membranes have a better phosphate adsorption capacity, their synthesis is much more complex and relies on expensive membrane support (Furuya et al., 2017).

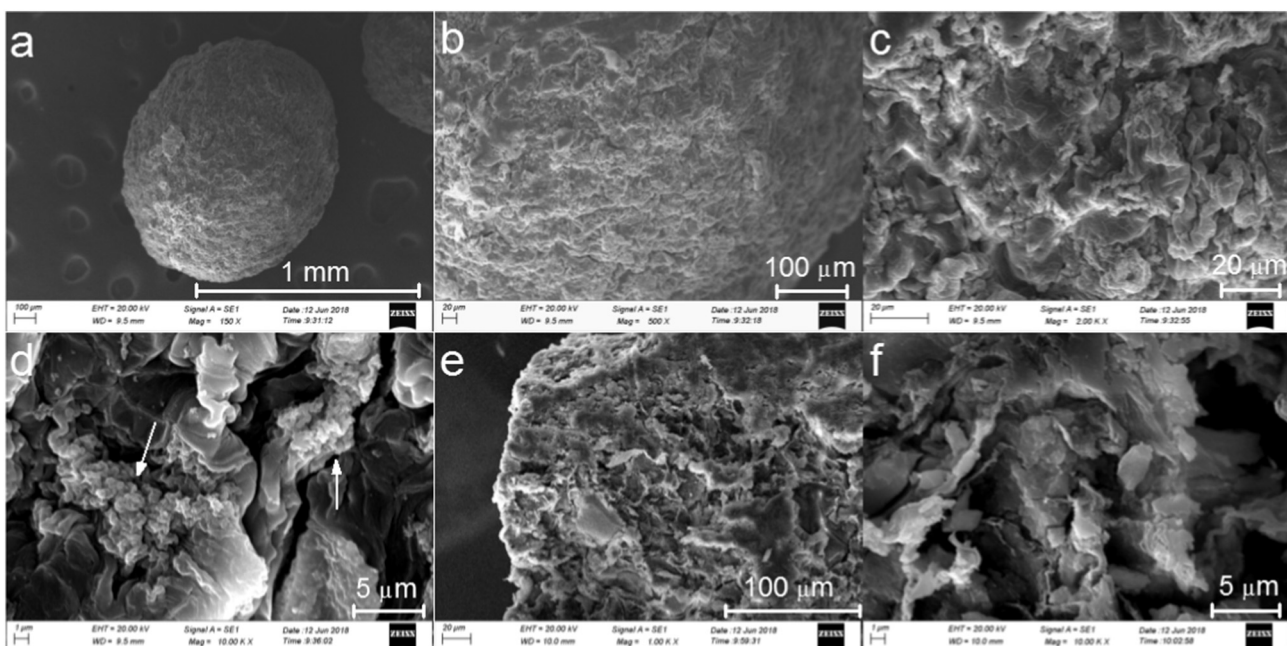


Fig. 3. SEM images of the surface (a–d) and cross section (e, f) of dried ZrA gel beads.

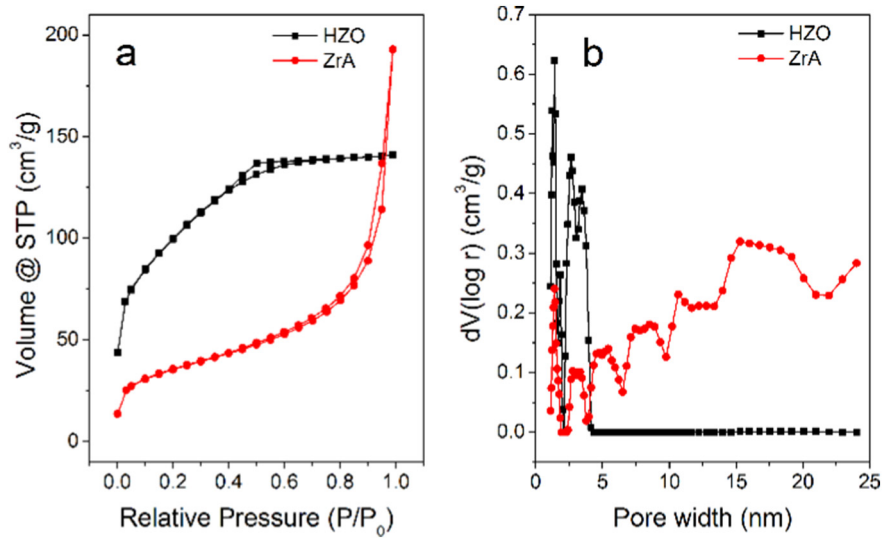


Fig. 4. HZO and ZrA N₂ adsorption/desorption isotherms (a) and pore size distributions (b).

3.4. Adsorption kinetics of ZrA

A kinetic study was performed to evaluate the ZrA phosphate recovery speed in comparison to that of HZO. The results shown in Fig. S5 indicate that HZO can more quickly reach an adsorption equilibrium compared to ZrA. Both the kinetics can be better fitted using a pseudo-second order model ($R^2 > 0.99$) than a first-order (Figs. S6 and S7). The adsorption kinetic constant of HZO (0.811) is much bigger than that of ZrA (0.125), as shown in Table S1. The reason may be because of the steric-hindrance effect of the ALG gel framework, which generates additional mass transfer resistance. This problem may be relieved by using smaller ZrA beads.

3.5. Advantages of ZrA beads in preventing HZO nanoparticle mass loss

There is a consensus that nanoparticles are difficult to recycle because of their well-known Brownian motion and electrostatic repulsion. The as-synthesized HZO nanoparticles have a very small size of tens of nanometers (Fig. S1). Its recyclability will be a potential problem hindering its practical application. We dispersed HZO into water with vigorous stirring at a concentration of 0.1 g/L. Gravity sedimentation was used to recycle the adsorbents. After 2 h of natural sedimentation, in the case of HZO, ~90% of the supernatant was carefully discarded while the remaining dispersion was oven dried to recycle the HZO. The results indicate that the recycled HZO mass quickly decreased

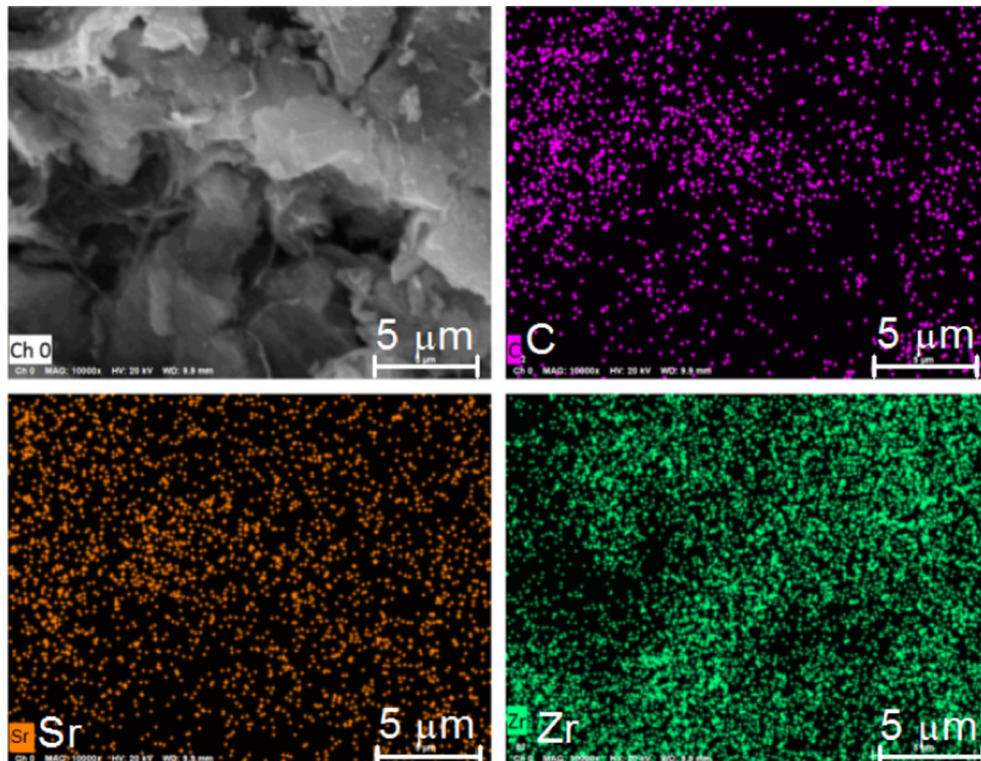


Fig. 5. EDX elemental mapping of C, Sr, and Zr in a cross section of ZrA gel beads.

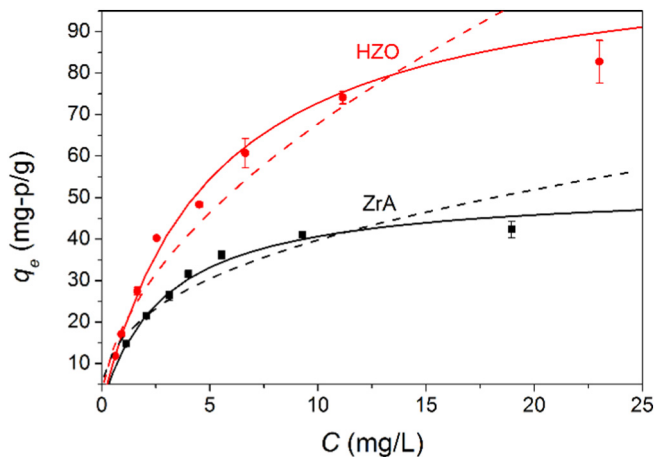


Fig. 6. HZO and ZrA gel bead adsorption isotherms. The solid and dashed lines are the Langmuir and Freundlich fitted curves of the isotherms, respectively.

Table 2
Langmuir and Freundlich fitting of the adsorption isotherms.

Sample	Langmuir			Freundlich		
	q_m (mg/g)	k_l (L mg ⁻¹)	R^2	$1/n$	k_f (L mg ⁻¹)(L mg ⁻¹) ^{1/n}	R^2
HZO	109.4	0.199	0.997	0.546	19.3	0.931
ZrA	52.5	0.344	0.993	0.384	16.4	0.870

after each cycle (Fig. 7). After five dispersion/recycle cycles, only ~43% could be recycled. The lost HZO will not only lead to a decrease in the phosphorus recycling efficiency and an increase in the cost of purchasing additional adsorbent but may also lead to a new environmental concern as a nano-pollutant. In the case of ZrA (0.1 g/L, dry mass concentration), all the ZrA beads precipitated to the bottom within seconds. There were basically no technical difficulties in the separation of the millimeter particles from the water by discarding the supernatant. After five cycles, nearly 100% of the ZrA beads were successfully recycled.

3.6. Advantages of ZrA beads against humic acid contamination

Surface water contains many types of natural macromolecules represented by humic acid (HA). HA is the residue of dead plants and animal bodies after natural degradation that can stably exist in water and soil for hundreds of years under natural conditions. HA is composed of many oxygen-containing groups (such as the carboxyl, aldehyde, hydroxyl, and phenolic hydroxyl groups) and nitrogen-containing groups (such as the amino, imine, and azacyclo groups) that can form stable

Table 3
Comparison of the phosphorus recovery capacities of various adsorbents.

Adsorbent	pH	q_m mg/g	Ref.
Zr-oxide, Hydrothermal	6.2	99.0	(Su et al., 2013)
Zr-hydroxide, commercial	7.1	18.5	(Johir et al., 2016)
ZnFeZr nanoparticles	7	20.3	(Schneider et al., 2017)
Zr/Fe modified carbon fiber	6.8	26.3	(Xiong et al., 2017)
Zr modified membrane	5	64.8	(Furuya et al., 2017)
HZO-loaded D201 resin	6.5	46.0	(Chen et al., 2015)
Zr/Fe modified 1402 resin	7	37.9	(Zhou et al., 2018)
AlOOH/biochar/ALG gel beads	6	48.8	(Jung et al., 2017)
Al-bentonite/ALG gel beads	7.8	11	(Pawar et al., 2016)
ZrA beads	7	52.5	This work

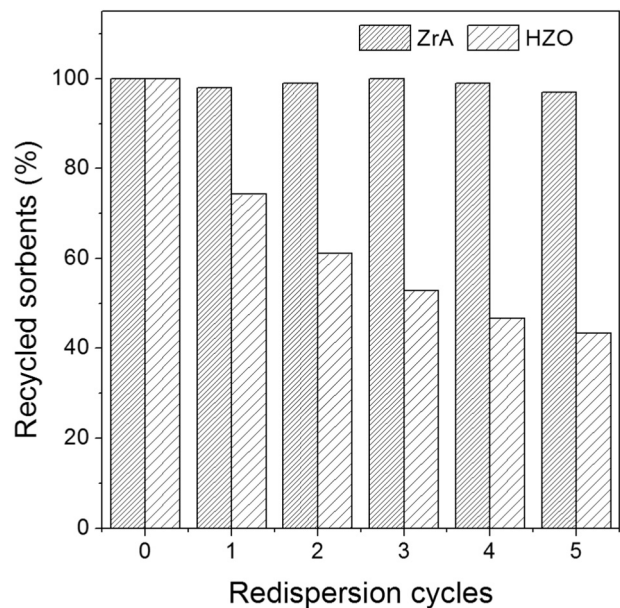


Fig. 7. Recycling of adsorbents.

complexes with metal ions and hydroxides. Therefore, HA may be adsorbed on HZO and, as a competition, decrease its phosphate adsorption capacity. We preloaded HA on HZO and ZrA by mixing these adsorbents (200 mg/L) into an HA solution (100 mg/L). After 24 h of stirring at room temperature, HZO were recycled and washed by water 3 times using a high-speed centrifuge. The HA-loaded HZO (HZO-HA) has a brown color (the inset of Fig. 8), indicating obvious intense adsorption of HA on HZO which can be further confirmed by the FTIR analysis (Fig. S8). Furthermore, in a comparative study with HZO, one can see that the HZO-HA phosphorus recovery efficiency is obviously suppressed as its recovery efficiency decreased from 98.7% (HZO) to 20.1%, as shown in Fig. 8.

The intense HA inhibition effect has to be considered for large-scale HZO phosphorus recovery applications because HA extensively occurs in natural aquatic environments. Regarding HA preloaded ZrA beads (ZrA-HA), only a weak influence can be observed as the recovery efficiency slightly decreased from 94.6 to 91.8%. The resistance of ZrA to

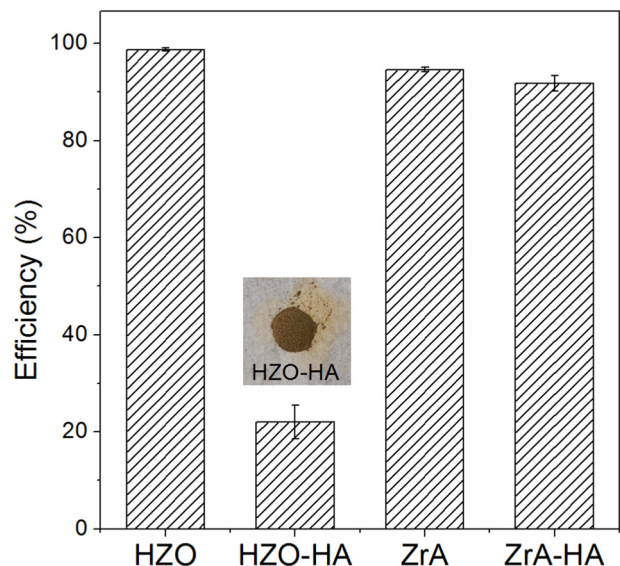


Fig. 8. Influence of humic acid (HA) contamination on phosphorus recovery. The inset is an optical image of HA-contaminated HZO ($C_0 = 10$ mg-P/L, $C_{ZrA} = 1.0$ g/L, and $t = 24$ h).

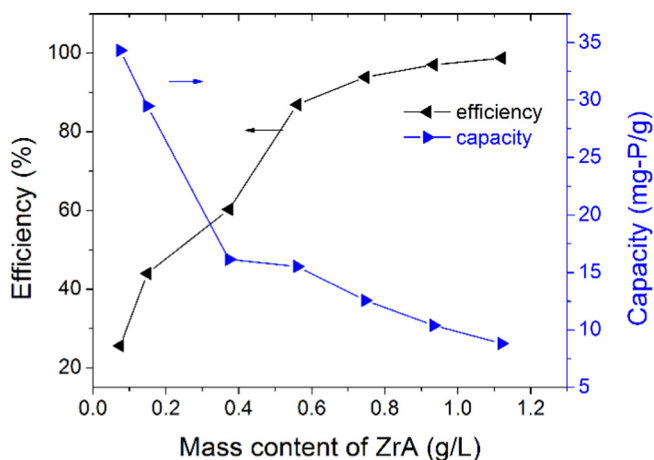


Fig. 9. Influence of the ZrA dosage on phosphorus recovery ($C_0 = 10$ mg-P/L, $C_{ZrA} = 1.0$ g/L, and $t = 10$ h).

HA contamination can be attributed to the steric-hindrance effect of the ALG polymer framework against HA. HA is a mixture of natural polymers with molecular weights mainly ranging from several thousands to hundreds of thousands. These macromolecules can be blocked from reaching the inside of ZrA and affecting the adsorption capacity of the HZO encapsulated within the ALG gel framework.

3.7. Performance of ZrA beads in simulated wastewater phosphate recovery

ZrA beads were used to treat artificial phosphate-containing wastewater with a low concentration of 10 mg-P/L. The results shown in Fig. 9 indicate that the phosphorus recovery efficiency quickly increased from 25.6 to 86.9% along with the increase in the ZrA mass concentration (C_{ZrA}) from 0.1 to 0.6 g/L. However, the efficiency only slowly increased after further increasing C_{ZrA} . The optimal ZrA dosage is proposed to be ~1.0 g/L as the residue phosphorus concentration is already lower than 0.5 mg-P/L, which is Standard A of the first class in “Discharge standard of pollutants for municipal wastewater treatment plant” of China (GB18918–2002).

3.8. Regeneration under an intense alkali condition

The adsorption capacity of ZrA is pH sensitive and can be inhibited under alkali conditions (Fig. S9). The phosphate-adsorbed ZrA was regenerated in 5 wt% NaOH. After five cycles of regeneration, ~80%

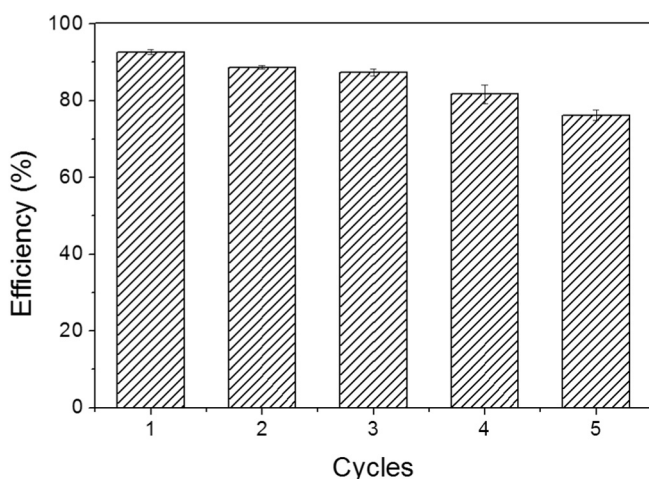


Fig. 10. Regeneration of ZrA gel beads ($C_0 = 10$ mg-P/L, $C_{ZrA} = 1.0$ g/L, and $t = 10$ h).

phosphorus recovery efficiency remained, which indicates good reuse properties that will dramatically decrease the material cost (Fig. 10). Even after overdue because of material aging, Zr and other soluble ions can be easily recycled via acid dissolution while residue alginate will precipitate as alginate acid which is a part of the alginate sodium production and purification process. As alginate is a type of bio-polymer material and environmentally benign, the whole ZrA life cycle is not likely to generate or release environmentally concerning pollutants. Regarding other adsorbents, such as an ionic exchange polymeric resin, they are essentially petrochemical products (Chen et al., 2015; Zhou et al., 2018). Their usage may possibly generate plastic fragments and particles after the end of their life cycle. As the size of the resin generally ranges from hundreds of micrometers to several millimeters, it will likely generate environmentally concerning microplastic pollutants that are an emerging environmental concern as potential new threats to aquatic ecosystems (Arias-Andres et al., 2018; Cole et al., 2011).

3.9. Economic cost analysis of raw materials for ZrA beads

A simple cost analysis was performed according to the chemical prices from Chemical Platform of the Chinese Academy of Sciences (CASmart). The results show that $SrCl_2$ is more expensive than $CaCl_2$ (Table 4). However, the main cost in producing ZrA is the purchase of $ZrOCl_2$ (80.7%) and alginate sodium (15%) while the cost of $SrCl_2$ is only 4.3% of the total cost. Using $SrCl_2$ instead of $CaCl_2$ will not lead to a significant increase in the total material cost. Moreover, using $SrCl_2$ as a crosslinking reagent is the only means to regenerate ZrA beads under an intense alkali condition (Table 1), which will significantly reduce the potential running cost of adsorbents. Therefore, using $SrCl_2$, rather than $CaCl_2$, to produce ZrA beads will be feasible for potential scale production.

4. Conclusion

Alkali resistant strontium alginate gel beads are successfully synthesized to immobilize HZO nanoparticles to produce ZrA gel beads for wastewater phosphate recovery. Sr^{2+} -crosslinked ZrA beads can endure an intense alkali condition, while other common ions, such as Ca^{2+} , Mg^{2+} , Fe^{3+} , Al^{3+} , and Zr^{4+} , cannot. ZrA beads have a high specific surface area (80.84 $m^2 \cdot g^{-1}$) and mesoporous structure (15.3 nm, 0.196 $cm^3 \cdot g^{-1}$), resulting in a high Langmuir adsorption capacity of 52.5 mg-P/g. Nearly 100% of the ZrA adsorbent can be recycled, and HZO mass loss is prevented. Furthermore, the strontium alginate gel framework protects the encapsulated HZO from adverse humic acid contamination to ensure a good phosphorus recovery performance, while naked HZO is subject to severe contamination and, in turn, has a dramatically decreased adsorption capacity. ZrA beads can be regenerated for at least 5 adsorption/desorption cycles. This work not only provides a novel, simple, and environmentally benign solution to realize efficient phosphate recovery but also implies possible applications of strontium alginate gel beads encapsulating other functional nanomaterials in numerous other applications.

Table 4
Cost analysis of ZrA bead raw materials.

	Alginate sodium	$SrCl_2$	$CaCl_2$	$ZrOCl_2$
Unit price (USD/kg) ^a	19.2	8.3	3.8	118
Mass (kg/kg-ZrA)	0.645	0.43		0.568
Unit cost (USD/kg-ZrA)	12.4	3.57		66.7
Cost percentage	15%	4.3%		80.7%

^a The prices are according to www.casmart.com.cn, 1 USD = 6.7744 CNY.

Acknowledgments

This research was supported by the National Natural Science Foundation of China (21701052), the Natural Science Foundation of Guangdong Province of China (32217073), the Special Funds for Basic Scientific Research Operations of Central Universities of China (21617323), Guangzhou Science and Technology Program (201804010401, China).

Declaration of competing interest

The authors declare no conflicts of interests.

Appendix A. Supplementary data

Supplementary data to this article can be found online at <https://doi.org/10.1016/j.scitotenv.2019.05.296>.

References

- Arias-Andres, M., Kettner, M.T., Miki, T., Grossart, H.P., 2018. Microplastics: new substrates for heterotrophic activity contribute to altering organic matter cycles in aquatic ecosystems. *Sci. Total Environ.* 635, 1152–1159.
- Awual, M.R., Jyo, A., Ihara, T., Seko, N., Tamada, M., Lim, K.T., 2011. Enhanced trace phosphate removal from water by zirconium(IV) loaded fibrous adsorbent. *Water Res.* 45 (15), 4592–4600.
- Chen, L., Zhao, X., Pan, B.C., Zhang, W.X., Hua, M., Lv, L., Zhang, W.M., 2015. Preferable removal of phosphate from seawater and wastewater by amorphous zirconium oxide-based nanocomposite of high stability. *J. Hazard. Mater.* 284, 35–42.
- Chitrakar, R., Tezuka, S., Sonoda, A., Sakane, K., Ooi, K., Hirotsu, T., 2006. Selective adsorption of phosphate from water using hydrous zirconium oxide-based amorphous zirconium hydroxide. *J. Colloid Interface Sci.* 297 (2), 426–433.
- Cole, M., Lindeque, P., Halsband, C., Galloway, T.S., 2011. Microplastics as contaminants in the marine environment: a review. *Mar. Pollut. Bull.* 62 (12), 2588–2597.
- Dechojarassri, D., Omote, S., Nishida, K., Omura, T., Yamaguchi, H., Furuichi, T., Tamura, H., 2018. Preparation of alginate fibers coagulated by calcium chloride or sulfuric acid: application to the adsorption of Sr²⁺. *J. Hazard. Mater.* 355, 154–161.
- Desmidt, E., Ghyselbrecht, K., Zhang, Y., Pinoy, L., Van der Bruggen, B., Verstraete, W., Rabaey, K., Meesschaert, B., 2015. Global phosphorus scarcity and full-scale P-recovery techniques: a review. *Crit. Rev. Environ. Sci. Technol.* 45 (4), 336–384.
- Dong, S.X., Wang, Y.L., Zhao, Y.W., Zhou, X.H., Zheng, H.L., 2017. La₃/La(OH)(3) loaded magnetic cationic hydrogel composites for phosphate removal: effect of lanthanum species and mechanistic study. *Water Res.* 126, 433–441.
- Du, W.Y., Li, Y.R., Xu, X., Shang, Y.N., Gao, B.Y., Yue, Q.Y., 2019. Selective removal of phosphate by dual Zr and La hydroxide/cellulose-based bio-composites. *J. Colloid Interface Sci.* 533, 692–699.
- Everaert, M., Warrinier, R., Baken, S., Gustafsson, J.P., De Vos, D., Smolders, E., 2016. Phosphate-exchanged mg-Al layered double hydroxides: a new slow release phosphate fertilizer. *ACS Sustain. Chem. Eng.* 4 (8), 4280–4287.
- Fang, L.P., Shi, Q.T., Nguyen, J., Wu, B.L., Wang, Z.M., Lo, I.M.C., 2017. Removal mechanisms of phosphate by lanthanum hydroxide nanorods: investigations using EXAFS, ATR-FTIR, DFT, and surface complexation modeling approaches. *Environ. Sci. Technol.* 51 (21), 12377–12384.
- Fang, L.P., Liu, R., Li, J., Xu, C.H., Huang, L.Z., Wang, D.S., 2018. Magnetite/lanthanum hydroxide for phosphate sequestration and recovery from lake and the attenuation effects of sediment particles. *Water Res.* 130, 243–254.
- Fernando, I.P.S., Kim, D., Nah, J.W., Jeon, Y.J., 2019. Advances in functionalizing fucoidans and alginates (bio)polymers by structural modifications: a review. *Chem. Eng. J.* 355, 33–48.
- Furuya, K., Hafuka, A., Kuroiwa, M., Satoh, H., Watanabe, Y., Yamamura, H., 2017. Development of novel polysulfone membranes with embedded zirconium sulfate-surfactant micelle mesostructure for phosphate recovery from water through membrane filtration. *Water Res.* 124, 521–526.
- Johir, M.A.H., Pradhan, M., Loganathan, P., Kandasamy, J., Vigneswaran, S., 2016. Phosphate adsorption from wastewater using zirconium (IV) hydroxide: kinetics, thermodynamics and membrane filtration adsorption hybrid system studies. *J. Environ. Manag.* 167, 167–174.
- Jung, K.W., Jeong, T.U., Choi, J.W., Ahn, K.H., Lee, S.H., 2017. Adsorption of phosphate from aqueous solution using electrochemically modified biochar calcium-alginate beads: batch and fixed-bed column performance. *Bioresour. Technol.* 244, 23–32.
- Kumar, P.S., Prot, T., Korving, L., Keesman, K.J., Dugulan, I., van Loosdrecht, M.C.M., Witkamp, G.J., 2017. Effect of pore size distribution on iron oxide coated granular activated carbons for phosphate adsorption - importance of mesopores. *Chem. Eng. J.* 326, 231–239.
- Kumar, R., Kim, S.J., Kim, K.H., Lee, S.H., Park, H.S., Jeon, B.H., 2018. Removal of hazardous hexavalent chromium from aqueous phase using zirconium oxide-immobilized alginate beads. *Appl. Geochem.* 88, 113–121.
- Kwon, O.H., Kim, J.O., Cho, D.W., Kumar, R., Baek, S.H., Kurade, M.B., Jeon, B.H., 2016. Adsorption of As(III), As(V) and Cu(II) on zirconium oxide immobilized alginate beads in aqueous phase. *Chemosphere* 160, 126–133.
- Li, R.H., Wang, J.J., Zhou, B.Y., Zhang, Z.Q., Liu, S., Lei, S., Xiao, R., 2017. Simultaneous capture removal of phosphate, ammonium and organic substances by MgO impregnated biochar and its potential use in swine wastewater treatment. *J. Clean. Prod.* 147, 96–107.
- Loganathan, P., Vigneswaran, S., Kandasamy, J., Bolan, N.S., 2014. Removal and recovery of phosphate from water using sorption. *Crit. Rev. Environ. Sci. Technol.* 44 (8), 847–907.
- Mayer, B.K., Baker, L.A., Boyer, T.H., Drechsel, P., Gifford, M., Hanjra, M.A., Parameswaran, P., Stoltzfus, J., Westerhoff, P., Rittmann, B.E., 2016. Total value of phosphorus recovery. *Environ. Sci. Technol.* 50 (13), 6606–6620.
- Othman, A., Dumitrescu, E., Andreescu, D., Andreescu, S., 2018. Nanoporous sorbents for the removal and recovery of phosphorus from eutrophic waters: sustainability challenges and solutions. *ACS Sustain. Chem. Eng.* 6 (10), 12542–12561.
- Pan, B.C., Li, Z.G., Zhang, Y.Y., Xu, J.S., Chen, L., Dong, H.J., Zhang, W.M., 2014. Acid and organic resistant nano-hydrated zirconium oxide (HZO)/polystyrene hybrid adsorbent for arsenic removal from water. *Chem. Eng. J.* 248, 290–296.
- Pawar, R.R., Gupta, P., Lalhmunsima, Bajaj, H.C., Lee, S.M., 2016. Al-intercalated acid activated bentonite beads for the removal of aqueous phosphate. *Sci. Total Environ.* 572, 1222–1230.
- Prabhu, S.M., Meenakshi, S., 2015. Novel one-pot synthesis of dicarboxylic acids mediated alginate-zirconium biopolymeric complex for defluoridation of water. *Carbohydr. Polym.* 120, 60–68.
- Qiu, H., Liang, C., Zhang, X.L., Chen, M.D., Zhao, Y.X., Tao, T., Xu, Z.W., Liu, G., 2015. Fabrication of a biomass-based hydrous zirconium oxide nanocomposite for preferable phosphate removal and recovery. *ACS Appl. Mater. Interfaces* 7 (37), 20835–20844.
- Schneider, M., Drenkova-Tuhtan, A., Szczerba, W., Gellermann, C., Meyer, C., Steinmetz, H., Mandel, K., Sextl, G., 2017. Nanostructured ZnFeZr oxyhydroxide precipitate as efficient phosphate adsorber in waste water: understanding the role of different material-building-blocks. *Environ. Sci. Nano* 4 (1), 180–190.
- Shroff, P., Parikh, S., Smt, S.M., 2018. Production and Characterization of Alginate Extracted from *Paenibacillus Riograndensis*. *Life Science Informatics Publications* <https://doi.org/10.26479/2018.0406.44>.
- Su, Y., Cui, H., Li, Q., Gao, S.A., Shang, J.K., 2013. Strong adsorption of phosphate by amorphous zirconium oxide nanoparticles. *Water Res.* 47 (14), 5018–5026.
- Tarayre, C., De Clercq, L., Charlier, R., Michels, E., Meers, E., Camargo-Valero, M., Delvigne, F., 2016. New perspectives for the design of sustainable bioprocesses for phosphorus recovery from waste. *Bioresour. Technol.* 206, 264–274.
- Xiong, W.P., Tong, J., Yang, Z.H., Zeng, G.M., Zhou, Y.Y., Wang, D.B., Song, P.P., Xu, R., Zhang, C., Cheng, M., 2017. Adsorption of phosphate from aqueous solution using iron-zirconium modified activated carbon nanofiber: performance and mechanism. *J. Colloid Interface Sci.* 493, 17–23.
- Ye, Y.Y., Ngo, H.H., Guo, W.S., Liu, Y.W., Li, J.X., Liu, Y., Zhang, X.B., Jia, H., 2017. Insight into chemical phosphate recovery from municipal wastewater. *Sci. Total Environ.* 576, 159–171.
- Zhang, X.L., Zhang, L., Li, Z.X., Jiang, Z., Zheng, Q., Lin, B., Pan, B.C., 2017. Rational design of antifouling polymeric nanocomposite for sustainable fluoride removal from NOM-rich water. *Environ. Sci. Technol.* 51 (22), 13363–13371.
- Zhou, K., Wu, B.R., Su, L.H., Xin, W.S., Chai, X.L., 2018. Enhanced phosphate removal using nanostructured hydrated ferric zirconium binary oxide confined in a polymeric anion exchanger. *Chem. Eng. J.* 345, 640–647.
- Zhu, X.D., Liu, Y.C., Qian, F., Shang, H., Wei, X.C., Zhang, S.C., Chen, J.M., Ren, Z.Y.J., 2018. Carbon transmission of CO₂ activated nano-MgO carbon composites enhances phosphate immobilization. *J. Mater. Chem. A* 6 (8), 3705–3713.